Simulation-Compatible Capacitive Coupler Modeling and Analysis for Wireless Power Transfer Applications

Ilya Zeltser

Ordnance Systems Division
Rafael Advanced Defense Systems Ltd.
P.O. Box 2250, Haifa 3102102, Israel
ilyaz@rafael.co.il
http://www.rafael.co.il

Eli Abramov

The Center for Power Electronics and Mixed-Signal IC, Department of Electrical and Computer Engineering
Ben-Gurion University of the Negev
P.O. Box 653, Beer-Sheva 8410501, Israel
eliab@post.bgu.ac.il
http://www.ee.bgu.ac.il

Mor. M. Peretz, *Member, IEEE*

The Center for Power Electronics and Mixed-Signal IC, Department of Electrical and Computer Engineering
Ben-Gurion University of the Negev
P.O. Box 653, Beer-Sheva 8410501, Israel
morp@ee.bgu.ac.il
http://www.ee.bgu.ac.il

***Abstract* - This study examines and compares several electrical models of capacitive-couplers (CC), which are a fundamental unit in capacitive power transfer (CPT) systems, responsible for the power transfer between the transmitter and the receiver. The applicability and implementation of the models under study in static and dynamic simulation analyses are presented and discussed in detail. The study further explores a series (Thevenin) model of CC, which consists of a dependent voltage source in series with a capacitor, on both receiver and transmitter sides, and shows its advantages over other models in simplifying system analysis and dynamic simulations. The model has been verified by FEA simulations and by experiments. The experimental results are in a good agreement with the theoretical analysis and the simulations.**

Keywords – capacitive-coupler modeling, capacitive power transfer, simulation-compatible models, wireless power transfer

I. Introduction

Capacitive-based wireless power transfer technology is being studied with much faster pace over the last decade, making it mature enough to be integrated into various appliances with output power ranging from milliwatts to kilowatts, such as: electric vehicles, biomedical implants, in-track-moving-systems, LED drivers and many more [1]-[3]. One of the main advantages of Capacitive Power Transfer (CPT) systems over their Inductive Power Transfer (IPT) counterparts, is the reduced sensitivity to metal objects interferences, due to the absence of Eddy currents [4]-[6]. In addition to efficiency improvements, CPT technology offers low-cost, low-weight and simpler end-to-end system construction [6]-[10]. In order to achieve better power transfer characteristics and improve the overall power transfer efficiency in capacitive WPT systems, high-frequency resonant conversion is employed, typically, in the range of several MHz.

A simplified block diagram of a descriptive CPT system is shown in Fig. 1. It consists of a high-frequency inverter in the transmitter's unit and a high-frequency rectifier on the receiver's side. In addition, similar to IPT systems, reactive matching networks in both the transmitting and the receiving units are used between the transmitter and the receiver [11]-[13]. The core element of CPT systems is the Capacitive-Coupler (CC), through which the energy is transferred by an electric field from the transmitter to the receiver. The CC interface is typically constructed using two pairs of conductive coupling plates (Fig. 1), such as copper foils or aluminum sheets [6], [10], [14]. The resulting coupling capacitances primarily depend on the area of the plates, distance, and the dielectric material between the plates [6], [10], [15]-[17], which in turn are chosen according to the application requirements.

Apparently, neither the analysis, nor the design of CPT systems are possible without an accurate model of the CC. Various CC models have been extensively discussed in prior art [6], [7], [18]-[23]. However, these models are either limited for specific geometry or lack the discussion about their applicability to different simulation analyses as well as a breakdown of pros and cons regarding the design and optimization of practical CPT systems.

The objective of this study is, therefore, to overview and compare several analytical and simulation-compatible models, that enable visualization and evaluation of CPT system under (and through) variations of the system parameters. It is shown that proper choice of a CC model enables significant simplification of static and dynamic analyses of the entire CPT. It is a further objective of this study to show the benefits of applying the series (Thevenin) model in CC analysis through a CPT case study.

II. Review: Capacitive-Coupler Modeling

Various arrangements of the CC have been thoroughly discussed in the prior art [6], [10], [20], [22]. To establish definitions that are used throughout the paper and for sake of clarity, the essential details are briefly reviewed. A typical CC configuration is shown in Fig. 1, whereas its simplified, equivalent electrical circuit is depicted in Fig. 2. The circuit comprises six lumped capacitors [10], [22], [23], such that each of them represents the coupling between the corresponding plates of the CC in Fig. 1.

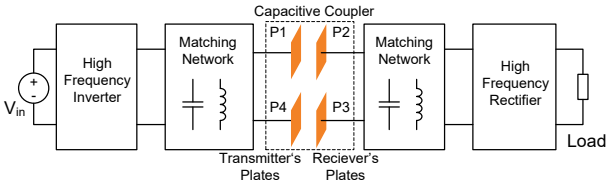

Fig. 1. Simplified block diagram of wireless CPT system with a conventional two-pair capacitive-coupler arrangement.

This work was supported by the Prof. A. Pazi Research Foundation

2022 IEEE Energy Conversion Congress and Exposition (ECCE) | 978-1-7281-9387-8/22/$31.00 ©2022 IEEE | DOI: 10.1109/ECCE50734.2022.9947874

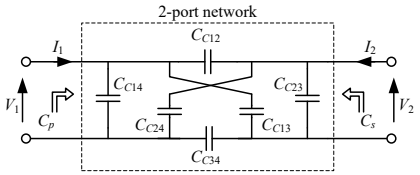

Fig. 2. Equivalent capacitances model of the CC.

Generally, the CC can be treated as a 2-port network with two inputs on the transmitter's side and two outputs on the receiver's side, as shown in Fig. 2 as well. The capacitors "seen" at the input and at the output of this 2-port network are denoted as C_p and C_s, respectively. Hence, the current and voltage relationships at the input and the output can be expressed as follows:

$$\begin{cases} I_1 = C_p \frac{dV_1}{dt} + C_{ps} \frac{dV_2}{dt} \\ I_2 = C_{sp} \frac{dV_1}{dt} + C_s \frac{dV_2}{dt} \end{cases} \quad (1)$$

where I_1, I_2, V_1, and V_2, are input and output currents and voltages, and $-C_{ps} = -C_{sp}$ is the mutual capacitance, C_m. Solving the Kirchhoff equations at the input and at the output yields [10], [22]-[24]:

$$\begin{cases} C_p = C_{C14} + \frac{(C_{C12}+C_{C13})\cdot(C_{C42}+C_{C43})}{C_{C12}+C_{C13}+C_{C42}+C_{C43}} \\ C_s = C_{C23} + \frac{(C_{C12}+C_{C42})\cdot(C_{C13}+C_{C43})}{C_{C12}+C_{C13}+C_{C42}+C_{C43}} \\ C_m = \frac{C_{C43}C_{C12}-C_{C13}C_{C42}}{C_{C12}+C_{C13}+C_{C42}+C_{C43}} \end{cases} \quad (2)$$

Similarly, to an inductive-based coupler, the coupling coefficient between the input and the output is expressed as

$$k_{CC} = \frac{C_m}{\sqrt{C_p C_s}}. \quad (3)$$

According to (1), a few possible CC models are devised and detailed in the following subsections.

A. π-Model

Eq. (1) can be rewritten in the following form:

$$\begin{cases} I_1 = (C_p - C_m)\frac{dV_1}{dt} + C_m \frac{d}{dt}(V_1 - V_2) \\ I_2 = C_m \frac{d}{dt}(V_2 - V_1) + (C_s - C_m)\frac{dV_2}{dt} \end{cases} \quad (4)$$

which can be further represented as a π-model, shown in Fig. 3 [7], [10], [22]. This model can be applied to any circuit simulation platform without any modifications. However, in this model, all three capacitors depend on the coupling capacitance C_m, meaning that the model needs to be recalculated every time the receiver and the transmitter move with respect to each other. As a result, using this model for dynamic analysis of CPT systems is rather complex and cumbersome.

A. Parallel (Norton) Model

The input and the output currents in eq. (1), are given by a sum of two capacitive currents, which can be translated to electrical circuitry representation as delineated in Fig. 4.

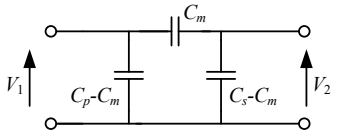

Fig. 3. π –model of CC.

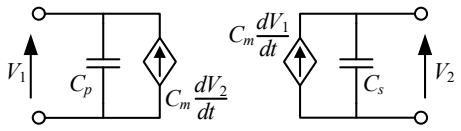

Fig. 4. parallel (Norton) model of CC.

The voltage-dependent current sources in Fig. 4 can be implemented, for instance, by a behavioral model (such as EVALUE in SPICE) where {*expression*} is defined as a derivative of V_1 or V_2 times C_m. This is demonstrated in Fig. 5 for SPICE compatible simulators, where the derivatives of V_1 and V_2 are calculated by applying SPICE's built-in function 'DDT' (time derivative). It should be emphasized however, that due to the use of the function 'DDT', the implementation of this simulation-compatible model is only valid for time-domain analysis. An alternative method to facilitate the derivative function is by a passive RC network or differentiator using active amplification stage. These methods are compatible with SPICE's ac analysis, however, an additional root, at relatively low frequency, is introduced to the system dynamics.

Another simulation-compatible approach for the parallel (Norton) model is depicted in Fig. 6. There, the capacitive currents of voltage-dependent current sources on the transmitter and receiver sides are generated by exposing two auxiliary capacitors, C_{aux1} and C_{aux2} of 1F to the voltages V_2 and V_1, respectively ([25], [26]). Then, their current is sensed and multiplied by C_m using the current sources I_{cm1} *and* I_{cm2} (see Fig. 6). This modeling approach is applicable in both frequency and time domain analyses. However, it involves relatively complex behavioral models that may give rise to conversion problems.

B. Series (Thevenin) Model

A further modification of the circuit model presented earlier is done by applying the Thevenin theorem to the left and to the right parts of Fig. 4. This yields dependent voltage sources in series with capacitors $C_{p/s}$, as shown in Fig. 7 [22], [27], [28]. In this case, the derivative is not required, the outputs of the dependent voltage sources are determined by a simple expression with basic arithmetic operators, thus, the series model can be implemented as is in any simulation platform.

Fig. 8 shows the implementation of the series model in two popular simulation platforms – PSpice and PSIM. In PSpice implementation (Fig. 8a) the input and the output voltages are constructed by series connection of the capacitors C_1 and C_2 with the dependent voltage sources E_1 and E_2 in accordance (the capacitors' values, C_p and C_s, are defined as global variables). C_m is emulated by the voltage which is set by the output of the dependent voltage source E_3. This voltage (V(Cm)) is then used in the expressions of E_1 and E_2 which are defined according to Fig. 7.

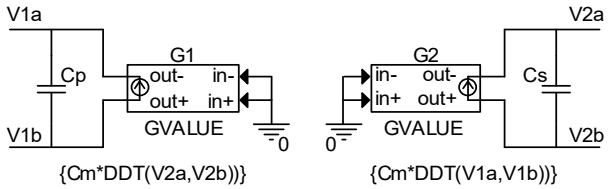

Fig. 5. SPICE compatible implementation of the Norton model using built-in 'DDT' function.

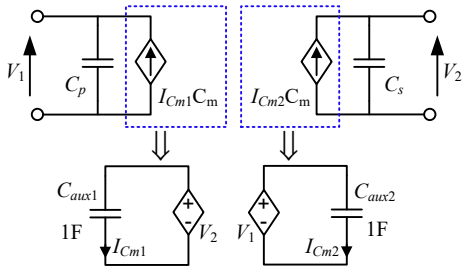

Fig. 6. Simulator compatible implementation of the Norton model by using auxiliary capacitors.

Similarly, in PSIM implementation (Fig. 8b), V_3 and V_4 are used as dependent voltage sources and their behavior is controlled by the computational blocks F_1 and F_2. Both of them have two inputs: first input (x1) is fed from a differential amplifiers AMP1 and AMP2 that sense the voltages V_1 and V_2, respectively; second input (x2) is connected to voltage node '*Cm*', which emulates the coupling capacitance C_m and determined by the computational block F_3.

Aside from the traditional time-domain simulation run where the 'end-time' (e.g., TSTOP - simulation time period) is defined explicitly, some simulation platforms offer a 'free-run' mode, where the simulation does not end until it is manually interrupted. In this mode, the user can change a variety of the circuit's parameters during the simulation run while examining the circuit's waveforms. This might be a useful way to examine the system's response to mutual capacitance variations. In PSIM platform, for example, it can be done by replacing the block F_3 in Fig. 8b with a DC voltage source, setting its magnitude to the value of the expected mutual capacitance C_m and changing it, then, during the simulation run.

III. Applying "Series" Thevenin Model to Analytical Analysis of a CPT System

Following the observations made in the previous section, a capacitively-coupled power transfer system of Fig. 1 with double-sided LC matching network [8], [10] is analyzed. The schematic diagram of the full system is shown in Fig. 9. The system comprises a full-bridge inverter at the front-end (Q_1-Q_4), which is operated at a switching frequency, f_{SW}, LC matching networks L_{m1}, C_{m1}, and L_{m2}, C_{m2}, a capacitive coupler, an output rectifier D_1-D_4 and a load R_L. It is assumed that both the matching networks are tuned to f_{SW}.

The matching networks are usually designed to have a high-quality factor implying that the system's behavior can be analyzed using first harmonic approximation [29], as depicted in Fig. 10. V_p and V_s represent the first harmonics of the square waves V_{AB} and V_O; $Z_O=\frac{8}{\pi^2}R_L$. The magnitudes of V_p and V_s are $V_{pm}=4V_{in}/\pi$ and $V_{sm}=4V_{out}/\pi$, respectively. The capacitive coupler and the matching capacitors are represented in Fig. 10 by the series (Thevenin) model as discussed in Section II-C.

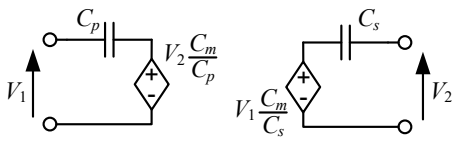

Fig. 7. Series (Thevenin) model of CC.

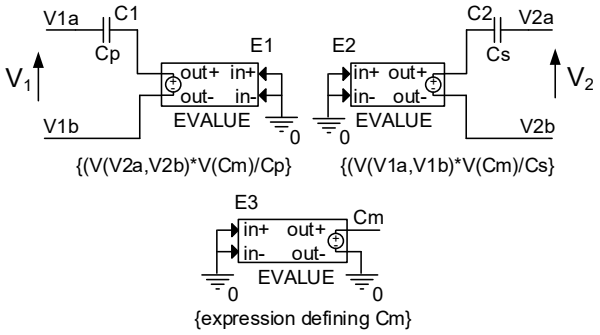

(a)

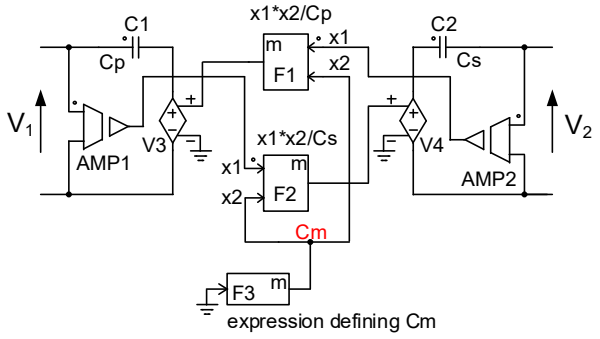

(b)

Fig. 8. CC series Thevenin model implementation in simulation platforms: (a) SPICE, (b) PSIM.

It should be noted that in the system of Fig. 9, the matching capacitors (C_{m1} and C_{m2}) are connected in parallel to the input and to the output of the capacitive coupler. Consequently, the capacitors C_1 and C_2 in the model of Fig. 10 are given by the sum of these matching capacitors and the capacitances C_p and C_s, 'seen' at the input and the output of the CC accordingly (see Fig. 9). That is, $C_1=C_{m1}+C_p$ and $C_2=C_{m2}+C_s$.

Now, both the transmitter and the receiver sides are modeled by a single branch, which significantly simplifies the analysis. For example, the output-to-input voltage ratio can be found intuitively, by inspection. Taking into consideration that such systems are operated at resonance [8]-[10], [14], [15], the relationship between V_p and V_2 is obtained as follows:

$$V_p = V_2 \frac{C_m}{C_1}. \tag{5}$$

V_2 can be found from the right branch of the circuit as follows (Fig. 10):

$$V_2 = V_s + \frac{V_s}{Z_o} Z_{Lm2} = V_s\left(1 + \frac{Z_{Lm2}}{Z_o}\right), \tag{6}$$

where $Z_{Lm2}=j\cdot 2\pi f_{sw}L_{m2}$. Substituting (6) into (5) yields:

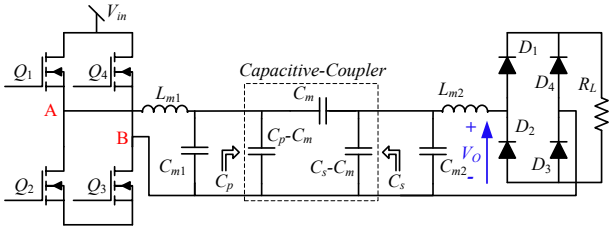

Fig. 9. Schematic diagram of capacitively-coupled WPT system with LC matching networks..

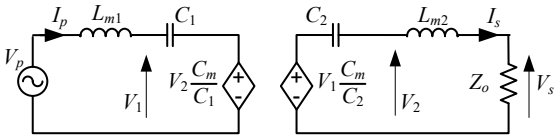

Fig. 10. Simplified equivalent circuit of the double-sided LC system using the Norton model.

$$\frac{V_s}{V_p} = \frac{C_1}{C_m} \cdot \frac{1}{1+jQ}, \tag{7}$$

where $Q = \frac{2\pi f_{sw} L_{m2}}{Z_0}$. The obtained result is in excellent agreement with the results of the analyses presented in the prior art [30], [31].

Another example would be finding the gyration ratio, that is, the relationship between the receiver's current and the voltage source at the transmitter. It can be achieved by expressing the voltage V_2 as a function of the current I_s ($V_2 = I_s(Z_{Lm2} + Z_o)$, see the right branch in Fig. 10) and substituting it into (5):

$$\frac{I_s}{V_p} = \frac{1}{Z_o(1+jQ)}. \tag{8}$$

The expression in (8) attests for current sourcing behavior (gyrator) of the system, again, as has been shown in the previous publications [30], [31].

IV. Series (Thevenin) CC's Model Verification

The series (Thevenin) model was verified by a Final Element Analysis (FEA) simulation and experimentally. It was done by applying a four 170x170mm copper plates CC to a system, shown in Fig. 9.

The system was simulated with two models of the CC - the lumped equivalent capacitance model (Fig. 2) and the series (Thevenin) model. The parameters of the lumped equivalent capacitance model were calculated by a FEA using MAXWELL, ANSYS. Fig. 11 shows the coupler's drawing used for the FEA.

Fig. 12 depicts simulation models of the system for both cases. The output of the input H-bridge is represented by a pulse voltage source E1 of magnitude V_{in}. The block 'U1' in Fig. 12a represents the lumped capacitance model of the coupler, and it serves as a link between the electrical and FEA analyses. The terminals P_1-P_4 are connected to the corresponding plates of the coupler (see Fig. 11). The simulations have been carried out in a Spice-compatible simulator (Ansys Twin Builder, former Simplorer). In this arrangement, when the simulation is started in the Twin Builder, it automatically engages an electrostatic FEA in MAXWELL that calculates the lumped capacitances of the coupler.

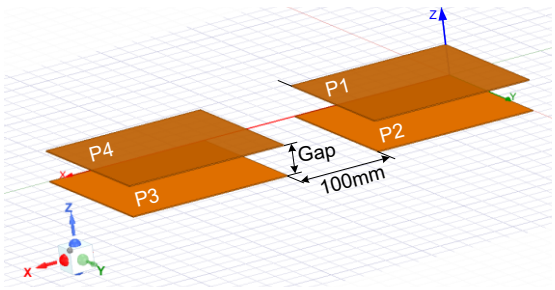

Fig. 11. FEA model of the capacitive-coupler.

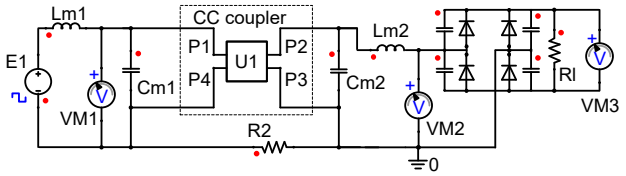

(a)

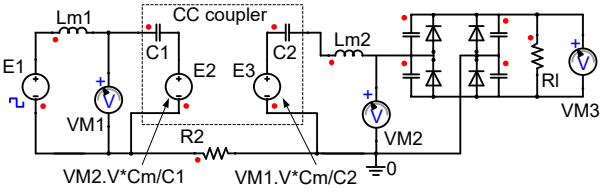

(b)

Fig. 12. Simulation model (Twin Builder, ANSYS) of the system of Fig. 9: (a) with lumped capacitances coupler's model, (b) with series (Thevenin) coupler's model.

Then, these capacitances are automatically fed into the model of Fig. 12a, and the simulation continues in the time-domain (transient analysis).

The series (Thevenin) model of the CC in Fig. 12b comprises two capacitors C_1 and C_2 and two voltage dependent sources E2 and E3. The magnitudes of the voltage sources are set according to Fig. 7. The coupling capacitance Cm and the capacitances C_1 and C_2 are calculated (off-line) from the lumped model parameters, by applying (2).

Fig. 13 shows the comparison of the system's key waveforms obtained with both models for 30mm gap. The input voltage is 30V and R_l is 15Ω. The matching networks are L_{m1}=L_{m2}≈67μH and C_{m1}=C_{m2}=156pF. As one can see, there is an excellent agreement between the results of the two models.

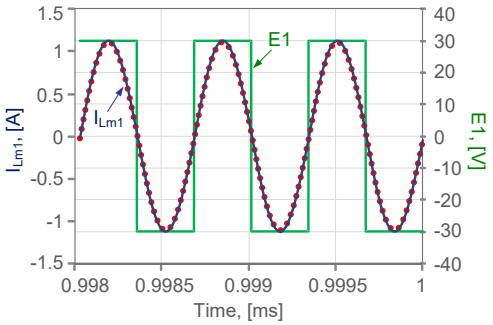

(a)

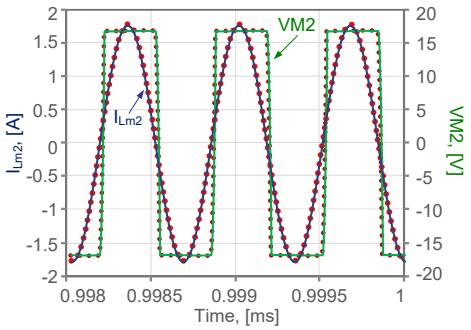

(b)

Fig. 13. Key waveforms simulation results: Solid lines – with lumped capacitance model; Dotted lines – with series (Thevenin) model. (a) Input, (b) Output.

Next, the simulation models of Fig. 12 were used to find the voltage and the gyration ratio of the system (using eq. (7) and (8)) when the coupler's gap was varied in the range of 20-70 mm. Fig. 14 shows the obtained results. Again, there is an absolute agreement between the models, validating the series (Thevenin) model.

The experimental prototype was constructed as shown in Fig. 15. The full-bridge inverter was implemented with GaN modules (LMG5200, 80V, 15 mΩ), and the gate drive signals were generated with a Cyclone IV FPGA. The switching frequency was set to 1.55MHz.

Fig. 16 shows experimental waveforms of the system for an air-gap of 30mm (corresponds to C_M ≈5pF approximately), whereas the input voltage V_{in}=30V and the load resistance R_{Load}=15Ω. Fig. 16a shows the transmitter waveforms of the prototype, and Fig. 16b shows the receiver waveforms. It can be noticed that there is a slight discrepancy between the FEA simulations and the experiments, this is due to imperfections of the coupler structure, imperfections of the resonators, and losses which were not taken into consideration in the simulations. Notwithstanding, the overall experimental results are in good agreement with the series (Thevenin) model for both simulation and theoretical predictions.

V. Discussion and Conclusion

This study has overviewed, evaluated, and compared three different models of the capacitive coupler in CPT systems: π-model, parallel (Norton), and series (Thevenin). The models have been devised by applying a generic method: first, treating the CC as a 2-port network and then deriving the characteristic equations from the circuit configurations. The study has also discussed the applicability of the models in different simulation analyses and platforms.

The π-model is the simplest and the most intuitive approach. Its main drawback relates to the lack of flexibility in evaluation of dynamic variations. It consists of three capacitors, where each must be modified to reflect misalignment and displacement of the system. This implies that for dynamic analysis of the system, these capacitors must be implemented by behavioral models, potentially complicating the overall circuit. Thus, in the context of dynamic analysis, the π-model is less attractive. However, it is a solid path for static analyses.

The parallel (Norton) model is a straightforward representation of the 2-port network's equations. Nevertheless, its implementation is quite cumbersome since it either involves a time derivative function, that limits the functionality of the model, or call for a more complex model were capacitive currents are generated by replicating the currents of two additional capacitors, using behavioral models.

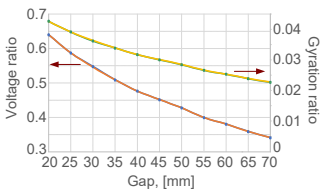

Fig. 14. CPT system parameters as function of the coupler's gap: Solid lines – with lumped capacitance model; Dotted lines – with series (Thevenin) model.

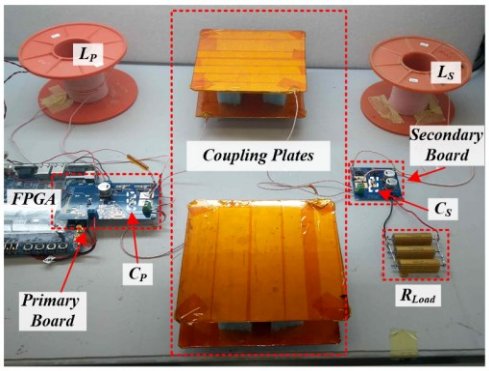

Fig. 15. Experimental setup of a capacitive WPT prototype.

Unlike the first two models, the series (Thevenin) model is applicable in its original form to time and frequency domain analyses, providing a generic solution in performing CPT system analysis. This is because, in this case, mutual capacitance, C_m, can be determined by a simple behavioral source or alike, which can be changed on-the-fly, helping to investigate the response of the system to its variations. To further demonstrate the benefits of this model, it has been used in analytical analysis of CPT system with a double- sided LC matching network, resulting in a simpler, more intuitive, equivalent circuit, which eases the understanding and prediction of the behavior of the CPT systems. The analytical analysis has been verified by simulation and experimentally. Excellent agreement has been found between the experimental, simulation, and analytical results.

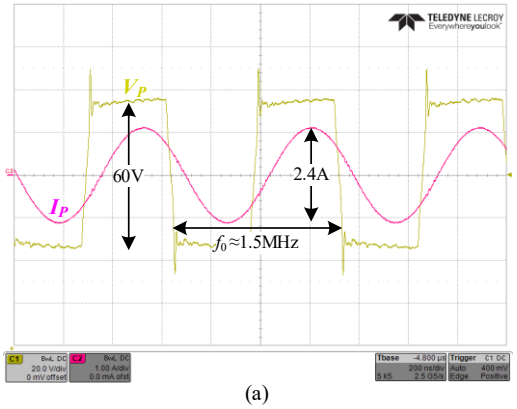

(a)

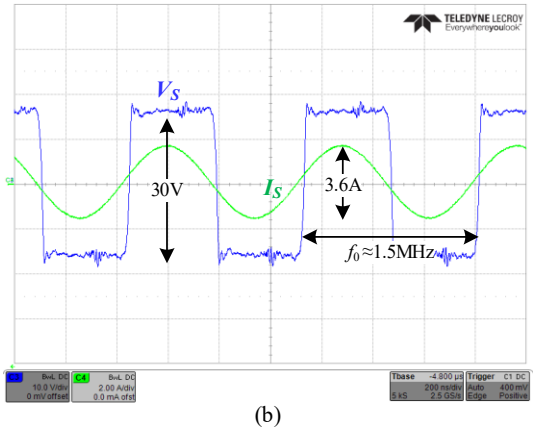

(b)

Fig. 16. Experimental waveforms with operating conditions: Vin =30 V, RLoad =15 Ω, coupling capacitance CM ≈5 pF. (a) Transmitter side V_P 20V/div, I_P 1A/div, (b) Receiver side V_S 10V/div, I_S 2A/div. Time scale 200ns/div.

REFERENCES

[1] S. Jaegue et al., "Design and implementation of shaped magnetic resonance-based wireless power transfer system for roadway-powered moving electric vehicles," IEEE Trans. Ind. Electron., vol. 61, no. 3, pp. 1179–1192, Mar. 2014.

[2] S.Y.R. Hui, W. Zhong and C.K. Lee, "A critical review of recent progress in mid-range wireless power transfer," IEEE Transactions on Power Electronics, vol. 29, no. 9, pp. 4500-4511, September 2014.

[3] F. Lu, H. Zhang, H. Hofmann, and C. Mi, "A double-sided LCLC compensated capacitive power transfer system for electric vehicle charging," IEEE Trans. Power Electron., vol. 30, no. 11, pp. 6011–6014, Jun. 2015.

[4] F. Musavi and W. Eberle, "Overview of wireless power transfer technologies for electric vehicle battery charging," *IET Power Electronics*, vol. 7, no. 1, pp. 60–66, 2014.

[5] C. Liu and A. P. Hu, ""Steady state analysis of a capacitively coupled contactless power transfer system," *in Proc. Energy Conversion Congress and Exposition, 2009. ECCE 2009*, pp. 3233-3238.

[6] M. P. Theodoridis, "Effective capacitive power transfer," *IEEE Trans. Power Electron*., vol. 27, no. 12, pp. 4906–4913, Dec. 2012.

[7] H. Zhang, F. Lu, H. Hofmann, W. Liu, and C. C. Mi, "A four-plate compact capacitive coupler design and LCL-compensated topology for capacitive power transfer in electric vehicle charging application," *IEEE Trans. Power Electron*., vol. 31, no. 12, pp. 8541–8551, Dec. 2016.

[8] F. Lu, H. Zhang, H. Hofmann, C. Mi, "A loosely coupled capacitive power transfer system with LC compensation circuit topology," *Proc. IEEE Energy Convers. Congr. Expo. (ECCE)*, pp. 1-5, 2016.

[9] F. Lu, H. Zhang, C. Mi, "A two-plate capacitive wireless power transfer system for electric vehicle charging Applications," *IEEE Trans. Power Electron*, vol. 33, no. 2, pp. 946-969, Aug. 2017.

[10] F. Lu, H. Zhang, H. Hofmann, and C. Mi, "A double-sided LC compensation circuit for loosely-coupled capacitive power transfer," *IEEE Trans. Power Electron*., vol. 33, no. 2, pp. 1633 – 1643, Feb. 2017.

[11] W. Zhang and C. Mi, "Compensation topologies for high power wireless power transfer systems," *IEEE Transactions on Vehicular Technology*, vol. 65, no.6, pp. 4768-4778, July 2015.

[12] S. Sinha, A. Kumar, S. Pervaiz, B. Regensburger and K.K. Afridi, "Design of efficient matching networks for capacitive wireless power transfer systems," *Proceedings of the IEEE Workshop on Control and Modeling for Power Electronics (COMPEL)*, Trondheim, Norway, June 2016.

[13] A. Kumar, S. Sinha, A. Sepahvand, K. K. Afridi, "Improved design optimization for high-efficiency matching networks," *IEEE Transactions on Power Electronics*, vol. 33, no. 1, pp. 37-50, Jan 2018.

[14] S. Sinha, A. Kumar, B. Regensburger, and K. K. Afridi, "A new design approach to mitigating the effect of parasitics in capacitive wireless power transfer systems for electric vehicle charging," *IEEE Trans. Transp. Electrific*., vol. 5, no. 4, pp. 1040–1059, Dec. 2019.

[15] B. Regensburger, J. Estrada, A. Kumar, S. Sinha, Z. Popović and K. K. Afridi, "High-performance capacitive wireless power transfer system for electric vehicle charging with enhanced coupling plate design," 2018 *IEEE Energy Conversion Congress and Exposition (ECCE)*, Portland, OR, 2018, pp. 2472-2477.

[16] L. Huang, A. P. Hu, A. K. Swain, and Y. Su, "Accurate steady-state modeling of capacitive-coupling interface of capacitive power transfer systems with cross-coupling," *Wireless Power Transfer*, vol. 3, no. 1, pp. 53–62, Mar. 2016.

[17] W. Zhou, Y. Su, L. Huang, X. Qing and A. P. Hu, "Wireless power transfer across a metal barrier by combined capacitive and inductive coupling," in *IEEE Transactions on Industrial Electronics*, vol. 66, no. 5, pp. 4031-4041, May 2019.

[18] J. Dai and D. C. Ludois, "Single active switch power electronics fork Kilowatt scale capacitive power transfer," in *IEEE Journal of Emerging and Selected Topics in Power Electronics*, vol. 3, no. 1, pp. 315-323, March 2015.

[19] A. Kumar, S. Pervaiz, Chieh-Kai Chang, S. Korhummel, Z. Popovic and K. K. Afridi, "Investigation of power transfer density enhancement in large air-gap capacitive wireless power transfer systems," *2015 IEEE Wireless Power Transfer Conference (WPTC)*, Boulder, CO, 2015, pp. 1-4.

[20] M. Kline, I. Izyumin, B. Boser, and S. Sanders, "Capacitive power transfer for contactless charging," in *Proc. IEEE Appl. Power Electron. Conf. Expo*., 2011, pp. 1398–1404.

[21] D. C. Ludois, J. K. Reed and K. Hanson, "Capacitive power transfer for rotor field current in synchronous machines," in *IEEE Transactions on Power Electronics*, vol. 27, no. 11, pp. 4638-4645, Nov. 2012.

[22] C. Liu, A.P. Hu, and M. Budhia, "A generalized coupling model for capacitive power transfer systems," *Proc. 36th Annual Conf. on IEEE Ind. Electron. Society*, Glendale, AZ, pp.274–279, Nov. 2010.

[23] L. Huang, A. P. Hu, A. K. Swain, and Y. Su, "Accurate steady-state modeling of capacitive-coupling interface of capacitive power transfer systems with cross-coupling," *Wireless Power Transfer*, vol. 3, no. 1, pp. 53–62, 2016.

[24] L. Huang and A. P. Hu, "Defining the mutual coupling of capacitive power transfer for wireless power transfer," in *Electronics Letters*, vol. 51, no. 22, pp. 1806-1807, 22 10 2015.

[25] I. Zeltser and S. Ben-Yaakov, "On SPICE simulation of voltage-dependent capacitors," in *IEEE Transactions on Power Electronics*, vol. 33, no. 5, pp. 3703-3710, May 2018.

[26] M. Evzelman and M.M Peretz, "Optimal design of a class-E resonant driver," *IET Power Electronics,* vol. 8, no.8, pp 1552-1557, Apr. 2015.

[27] E. Abramov, M. M. Peretz and I. Zeltser, "Soft-switching in capacitive-coupled wireless power transfer with LCLC compensation networks," *2020 IEEE Applied Power Electronics Conference and Exposition (APEC)*, New Orleans, LA, USA, 2020, pp. 3151-3158.

[28] S. Wang, J. Liang, H. Wang, and M. Fu, "An induced voltage source model for capacitive power transfer," *2020 IEEE Applied Power Electronics Conference and Exposition (APEC)*, New Orleans, LA, USA, 2020, pp. 846-851.

[29] R.L. Steigerwald, "A comparison of half-bridge resonant converter topologies," *IEEE Transactions on Power Electronics*, vol. 3, no. 2, pp. 174-182, April 1988.

[30] E. Abramov, J. M. Alonso and M. M. Peretz, "Analysis and behavioural modelling of matching networks for resonant-operating capacitive wireless power transfer," in *IET Power Electronics*, vol. 12, no. 10, pp. 2615-2625, Aug. 2019.

[31] E. Abramov, I. Zeltser, and M. M. Peretz, "Behavioral modeling of resonant power transfer systems with capacitive coupling: two-port network approach," *2019 IEEE Applied Power Electronics Conference and Exposition (APEC)*, Anaheim, CA, USA, 2019, pp. 3129-3136.